Available online at https://link.springer.com/journal/42241
http://www.jhydrodynamics.com
Journal of Hydrodynamics, 2024, 36(6): 1009-1020
https://doi.org/10.1007/s42241-025-0114-2

Large eddy simulation of the wake behind a sphere with and without density stratification at *Re* = 3 700

Gang Gao[1], Yang-jun Wang[2], Liu-shuai Cao[1*], De-cheng Wan[1]
1. *Computational Marine Hydrodynamics Lab (CMHL), School of Ocean and Civil Engineering, Shanghai Jiao Tong University, Shanghai 200240 China*
2. *College of Advanced Interdisciplinary Studies, National University of Defense Technology, Nanjing 210022, China*

(Received September 16, 2024, Revised October 20, 2024, Accepted October 21, 2024, Published online February 20, 2025)

Abstract: To enhance understanding of the flow characteristics around a sphere in both stratified and unstratified (UNS) fluids, large eddy simulations (LES) were conducted using a temperature-dependent density model at $Re = 3\,700$. The simulations were performed for flow around a sphere under UNS and stratified conditions $(Fr = 3)$. Horizontal and vertical vorticity, velocity, and streamline distributions were compared, and the evolution of vortex structures in the wake was analyzed. Furthermore, we quantified the velocity deficit, the root mean square (rms) of velocity components in all directions, and the turbulent kinetic energy (TKE) distribution. Additionally, the horizontal and vertical wake lengths were examined. The results demonstrate that the employed numerical simulation method accurately captures the behavior of stratified fluids, with outcomes in close agreement with experimental and numerical findings from previous studies. In the case of homogeneous fluid, a lower density value results in a faster decay of the velocity deficit. In stratified fluids, the vortex structures in the wake evolve through three distinct stages: 3-D, non-equilibrium (NEQ), quasi-two-dimensional (Q2D). For $x / D > 2$, the rms velocity in the vertical direction exceeds that in the other two directions. In UNS fluid, the TKE distribution forms a vertically elongated spindle shape, while in stratified fluid, it assumes an elliptical shape, being vertically compressed and horizontally expanded. The vertical extent of the density and density gradient distributions surpasses that of the wake.

Key words: Wake, sphere, unstratified (UNS) fluid, stratified fluid, velocity deficit, turbulent kinetic energy (TKE)

0. Introduction

Temperature and density stratification phenomena are commonly observed in solar ponds, reservoirs, river estuaries, the atmosphere, and shallow waters. When underwater vehicles operate in regions with thermal and density stratification, they generate complex turbulent and thermal wakes. These wakes are characterized by their extensive impact range, long persistence, and difficulty in elimination and camouflage. Consequently, they pose significant challenges to the stealth capabilities of underwater vehicles and are a crucial focus for current non-acoustic detection methods[1-3].

In the study of stratified fluid, the primary methods are experimental and numerical simulations. Regardless of the approach, two dimensionless parameters are critically important: The Reynolds number (Re) and the Froude number (Fr). The Reynolds number is defined as $Re = UD / \nu$, where U is the characteristic velocity, D is the characteristic velocity and ν is the kinematic viscosity. The Froude number is given by $Fr = U / ND$, where buoyancy frequency $N = \sqrt{-(g / \rho_0)(\partial\rho / \partial z)}$, g is the gravitational acceleration, ρ_0 is the reference density and $\partial\rho / \partial z$ as the density gradient in the vertical direction. The Froude number describes the strength of stratification, with smaller Fr indicating stronger stratification. The Reynolds number represents the ratio of inertial to viscous forces. The buoyancy time period (N_t) and the dimensionless length (x / D)

Project supported by the National Natural Science Foundation of China (Grant Nos. 52001210, 52131102).
Biography: Gang Gao (1999-), Male, Ph. D.,
E-mail: GC911741@sjtu.edu.cn
Corresponding author: Liu-shuai Cao,
E-mail: liushuaicao@sjtu.edu.cn

can be expressed as $N_t = x / FrD$.

Early experiments by Bonnier and Eiff[4] on linearly stable saltwater stratification proposed that wake evolution can be divided into four stages: 3-D near wake, collapse, transition zone, and finally far wake. Lin et al.[5-6], through experiments on linearly stratified fluid, measured the turbulent wake behind a sphere and concluded that the frequency of quasi-two-dimensional (Q2D) vortices in the far wake is determined by the vortex shedding frequency in the near wake, which is significantly influenced by stratification. Kim and Durbin.[7], in wind tunnel experiments, measured the vortex shedding frequency in sphere wakes across a Reynolds number in the range $500 < Re < 60\,000$. They studied the effects of acoustic excitation and discovered interactions between two frequency modes at lower Reynolds numbers, through this interaction, external forcing at unstable frequencies can alter the vortex shedding frequency. Xiang et al.[8-9] found that wake structures at high Re and low Fr are similar to those at low Re and high Fr, with increasing Re leading to greater wake instability.

With the advancement of computer technology, numerous researchers have undertaken significant work to achieve numerical simulations of density stratification. Huang et al.[10] proposed a temperature-driven density stratification model in STAR-CCM+. Wang et al.[11-12] developed a solver named "twoLiquidMixing_skin_Foam" in OpenFOAM. Nadaf et al.[13] utilized the fluid simulation solvers in OpenFOAM. Jacobs[14] improved buoyantPimpleFoam to simulate propeller rotation in stratified fluid. Chen et al.[15] implemented temperature and salinity stratification in Fluent through custom user-defined functions (UDFs).

Other researchers have achieved notable results by developing custom solvers to simulate stratified fluids. Rodríguez et al.[16-17] conducted direct numerical simulations of flow over a sphere, focusing on the instability of the shear layer and its impact on vortex structures and wake outcomes at $Re = 3\,700$, $Re = 10\,000$. Constantinescu et al.[18] studied subcritical and supercritical sphere wake fields across a wide range of Reynolds numbers (10^4-10^6), emphasizing pressure distribution, surface friction, and drag. Chongsiripinyo et al.[19-22] performed large eddy simulations (LES) at $Re = 50\,000$, $Fr = 50,\ 10,\ 2$, investigating uniform and stratified fluid past a disk. They found that in uniform fluid and at high Fr, the wake core turbulence is initially anisotropic. They also quantified turbulent kinetic energy (TKE) and entropy variance to assess the impact of stratification strength. Chongsiripinyo et al.[23] used direct numerical simulation (DNS) with temporal modeling to track stratified wakes far downstream, concluding that the vertical extent of density disturbances far exceeds the boundary region of the wake. Nadaf et al.[13] considered both linear and nonlinear density distributions and found that wakes tend to propagate horizontally under nonlinear density distributions, with the effective persistence time of the wake significantly increasing with Fr. Pal et al.[24-25], through DNS at $Re = 3\,700$, studied the wake of a sphere and observed that velocity deficit accelerates between $N_t = \pi$, $N_t = 2\pi$. They also found that the contributions of transport and buoyancy terms in the TKE calculations become increasingly significant with stronger stratification.

It can be observed that most numerical simulations of sphere wake fields rely on DNS, which is computationally expensive[26-29]. Furthermore, the understanding of the changes in physical phenomena between uniform and stratified fluids remains insufficient. Therefore, it is necessary to conduct numerical simulations of both uniform and stratified fluids at the same Reynolds number.

1. Numerical methods

1.1 *Governing equations*

This study utilizes the commercial software STAR-CCM+ 2023 for numerical simulations. In the solution process of this paper, the fluid motion satisfies the mass conservation and momentum conservation equations.

$$\nabla \cdot \boldsymbol{U} = 0 \tag{1}$$

$$\frac{\partial \rho \boldsymbol{U}}{\partial t} + \nabla \cdot (\rho \boldsymbol{U}\boldsymbol{U}) = -\nabla p + \rho \boldsymbol{g} + \nabla \cdot (\mu \nabla \boldsymbol{U}) \tag{2}$$

where $\boldsymbol{U}$ is the velocity field, ρ is the density of fluid, t is the time, p is the pressure field, $\boldsymbol{g}$ is the gravity acceleration and μ is the dynamic viscosity coefficient.

In the context of the Navier-Stokes equation for incompressible fluids, LES can be performed by applying a filter function to derive Eqs. (3), (4).

$$\frac{\partial u_i}{\partial x_i} = 0 \tag{3}$$

$$\frac{\partial u_i}{\partial t} + \frac{\partial u_i u_j}{\partial x_j} = -\frac{1}{\rho}\frac{\partial p}{\partial x_i} + \nu \frac{\partial^2 u_i}{\partial x_j x_j} - \frac{\partial \tau_{ij}}{\partial x_j} + f_i \tag{4}$$

The velocity vectors u_i, u_j $(i, j = 1, 2, 3)$ are filtered

to obtain their respective components in the x-direction, denoted by x_i, x_j. The variables τ_{ij}, f_i are the stress tensor at the subgrid scale (SGS), an exogenous term. The SGS model is used for approximate analysis of the anisotropic part.

$$\tau_{ij}^{a} = -\frac{2}{3}\delta_{ij}k_r \tag{5}$$

where δ_{ij} is the Kronecker function, k_r is the residual internal energy.

In the standard SGS model, the SGS eddy viscosity is approximated.

$$\nu_t = (C_S\Delta)^2\left|S_{ij}\right| \tag{6}$$

$$\left|S_{ij}\right| = \sqrt{2S_{ij}S_{ij}} \tag{7}$$

$$S_{ij} = \frac{1}{2}\left(\frac{\partial u_i}{\partial x_j} + \frac{\partial u_j}{\partial x_i}\right) \tag{8}$$

In this study, use C_S to represent the Smagorinsky constant, which has a fixed value of 0.1, Δ is used to denote the filter size, with grid unit sizes being equal and $\left|S_{ij}\right|$ is the rate at which the strain decomposition speed decreases after filtering. The viscosity is then employed to calculate the anisotropic subgrid stress tensor.

$$\tau_{ij}^{a} = -2\nu_t\overline{S_{ij}} \tag{9}$$

In order to realize the linear distribution of density, this paper needs to solve the energy equation, and realize the linear distribution of density by controlling the linear distribution of temperature.

$$\frac{\partial(\rho T)}{\partial t} + \nabla\cdot(\rho \boldsymbol{U} T) = \nabla\cdot\left(\frac{k}{c}\nabla T\right) + S_T \tag{10}$$

where $[\partial(\rho T)]/\partial t$ is the local change rate of the temperature field, $\nabla\cdot(\rho \boldsymbol{U} T)$ is the thermal convection term, $\nabla\cdot[(k/c)\nabla T]$ is the thermal diffusion term and S_T is the source term. Neglecting the influence of thermal radiation, expressing the density as a function of temperature, given the upper and lower temperature distributions of the layered area, the corresponding density distribution can be calculated.

1.2 *Computational conditions*

As shown in Fig. 1, D is the diameter of the sphere. In the setup of the computational domain, to prevent recirculation caused by proximity to the inlet, the inlet is placed $10D$ upstream of the sphere. To allow the wake to fully develop, the outlet is located $15D$ downstream of the sphere. To prevent interference with the wake from the sides of the computational domain, the lateral boundaries are positioned $15D$ away from the sphere on both sides. The upper and lower boundaries of the computational domain are $4D$ away from the sphere.

As illustrated in Fig. 2, the mesh is refined on the surface of the sphere and locally refined in the wake region behind the sphere. Regarding the boundary conditions, the inlet of the computational domain is set as a velocity inlet. Similarly, the lateral, upper, and lower boundaries are also set as velocity inlets. The outlet of the computational domain is set as an outflow condition.

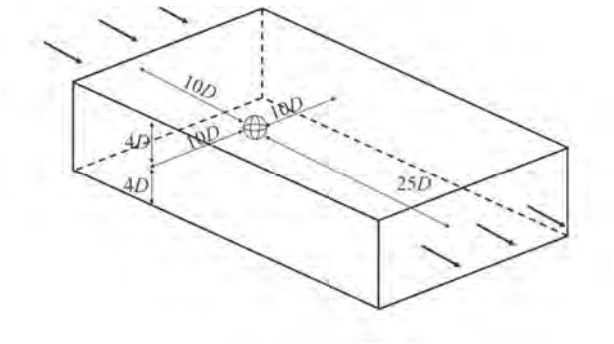

Fig. 1 The computational domain

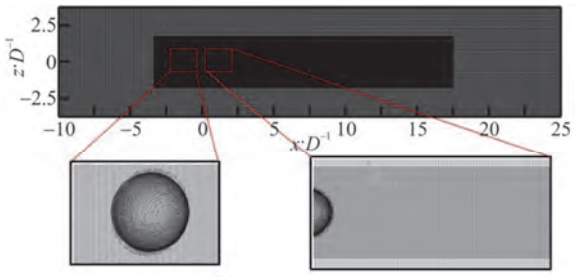

Fig. 2 (Color online) The computational mesh

2. Verification and validation

2.1 *Validation of the simulation method*

Since this study involves numerical simulations of both uniform and stratified fluids, we first conducted a validation of the methodology under uniform fluid condition. At $Re = 4\,200$, we primarily compared our results with those of Kim and Durbin[7], Rodriguez et al.[17] and Pal et al.[25]. As shown in Fig. 3, the pressure coefficient distribution on the surface of the sphere indicates that the trend and values of the pressure coefficient in a homogeneous fluid with

uniform density are close to those reported by other researchers. The pressure coefficient decreases monotonically in the range of $0<\theta<73$, and then gradually increases in the range of $73<\theta<180$. Figure 4 presents the normalized mean velocity distribution along the centerline of the wake, demonstrating that our results are very similar to those of Rodriguez et al.[17] Due to the formation of a recirculation zone behind the sphere, the streamwise velocity v_x/U is less than 0 for $x/D<3$. The findings in Figs. 3, 4 confirm the reliability of our numerical simulation methods in a homogeneous fluid with uniform density.

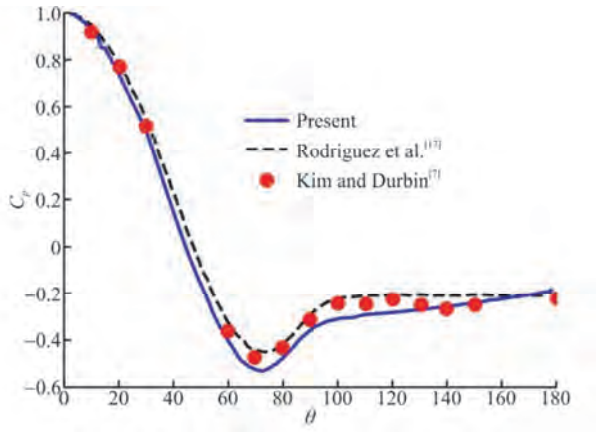

Fig. 3 (Color online) Mean pressure distribution (UNS)

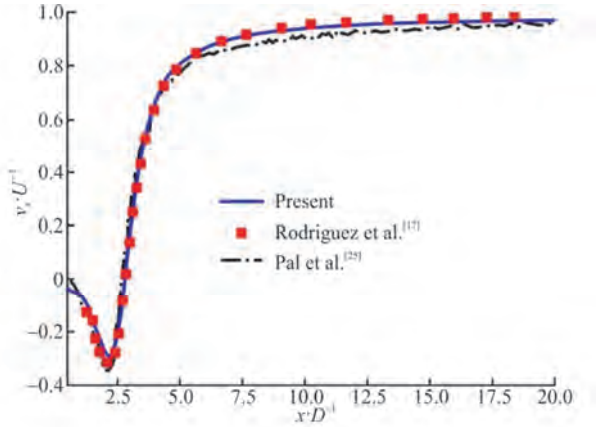

Fig. 4 (Color online) Streamwise evolution at the centreline of mean defect velocity (UNS)

Subsequently, we conducted validation under stratified fluid condition. At $Fr=3$, $Re=3\,700$, we primarily compared our results with those of Pal et al.[25], Nadaf et al.[13]. Although Bonnier et al.[4] performed experiments at $Re=6\,900$, $Fr=3$, we also used their results for reference. Figures 5, 6 present the normalized velocity deficit variation and the root mean square (rms) values of the streamwise velocity along the centerline of the wake. Since the Reynolds number in the experiments conducted by Bonnier et al.[4] was higher, their results show significantly greater values in both velocity deficit and the rms of the streamwise velocity compared with the present study and the results of Pal et al.[25]. For the mean velocity deficit, it can be seen that our results are closer to those of Pal et al.[25] compared with Nadaf et al.[13], And for the rms of the streamwise velocity, when $N_t>0.5$, the values and trends from the current study are closer to the results of Pal et al.[25] compared with those of Nadaf et al.[13], indicating the reliability of our stratified fluid simulation method.

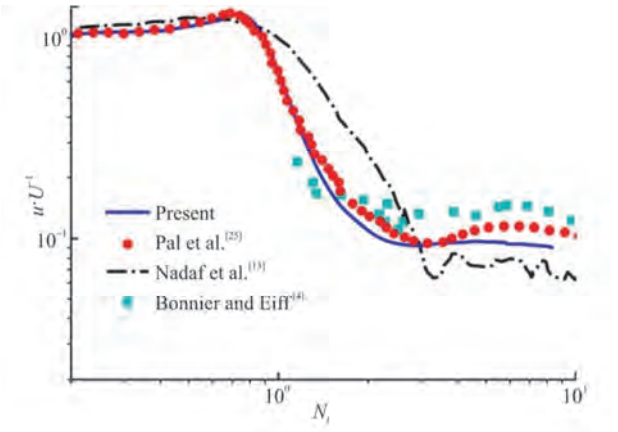

Fig. 5 (Color online) Streamwise evolution at the centreline of mean defect velocity ($Fr=3$)

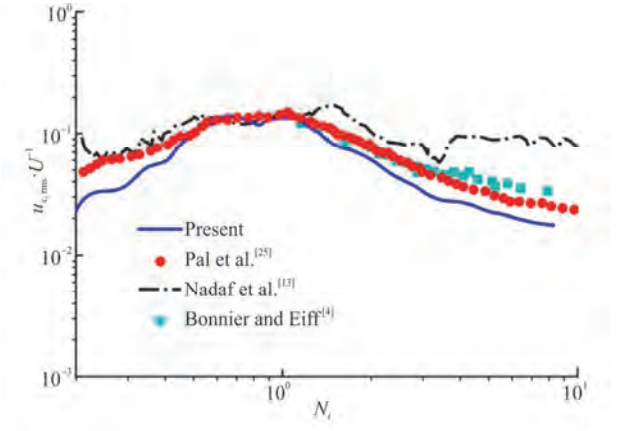

Fig. 6 (Color online) Streamwise evolution at the centreline of rms streamwise velocity ($Fr=3$)

2.2 *Grid independence study*

After completing the validation of the method, we conducted a grid sensitivity analysis. Based on different grid sizes, we set up three sets of grids: Coarse, medium, and fine, with grid counts of 6.85×10^6, 1.2×10^7, 2.1×10^7. Figure 7 shows the pressure coefficient distribution on the surface of the sphere for

different grids, indicating that the results are very close across different grid resolutions. Figure 8 presents the normalized mean velocity distribution for different grids, showing that the results from the medium grid are closer to those from the fine grid. To ensure the accuracy of the computational results while reducing computational costs, we used the medium-sized grid, with a grid count of 1.2×10^7.

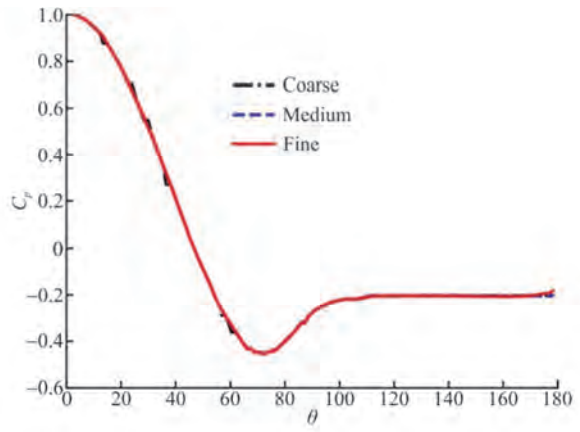

Fig. 7 (Color online) Mean pressure distribution at different grids

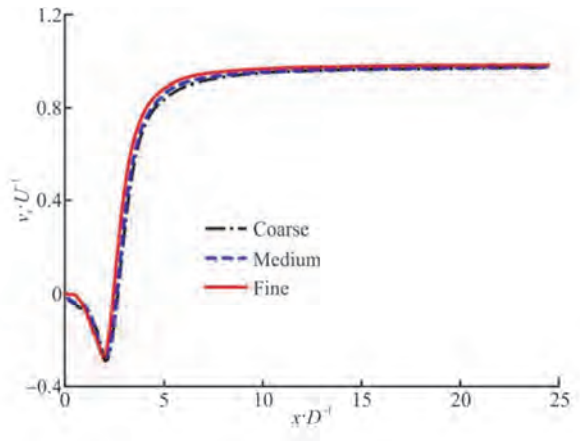

Fig. 8 (Color online) Streamwise evolution at the centreline of mean defect velocity at different grids

3. Results and discussion

As shown in Fig. 9, in a linearly stratified fluid, the density increases gradually from top to bottom along the vertical direction. The density of the fluid at the topmost part is defined as ρ_{top}, the density of the fluid in the middle of the computational domain is defined as ρ_{middel}, and the density of the fluid at the bottommost part is defined as ρ_{bottom}. Since we are conducting a comparative study between UNS and stratified fluid, it is necessary to determine the density of fluid for the UNS case as well, where the fluid is homogeneous. Therefore, we use ρ_{top}, ρ_{middel}, ρ_{bottom} as the densities for the UNS case.

Figure 10 shows the normalized velocity deficit curves along the centerline of the wake. Compared with the stratified fluid $(Fr = 3)$, the UNS results decay faster, indicating a broader and longer-lasting wake in stratified condition. Additionally, in the UNS case, the smaller the density of fluid $(\rho_{\text{top}} < \rho_{\text{middel}} < \rho_{\text{bottom}})$, the faster the velocity deficit curve decays. This indicates that the comparative pattern between homogeneous fluid with different densities and stratified fluid is consistent. For subsequent calculations and discussions, ρ_{middel} is set as the density for the homogeneous fluid.

Fig. 9 (Color online) Schematic of density in a linear stratification

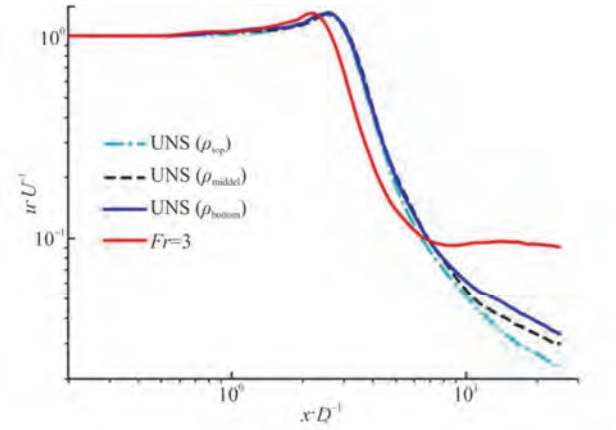

Fig. 10 (Color online) Streamwise evolution at the centreline of mean defect velocity

3.1 *Visualization of wake*

Figure 11 shows the vorticity, velocity, and streamline distributions under UNS condition. Compared with $Fr = 3$, the wake of the sphere does not experience suppression in the vertical direction under UNS condition. Due to the formation of a low-pressure region behind the sphere, which results in recirculation, the recirculation zone for the UNS fluid is primarily observed in the region $x / D < 2.5$, as shown by the vorticity, velocity, and streamline distributions in Fig. 11.

At $Fr = 3$, as shown in Fig. 12, the vorticity, velocity, and streamline distributions at different cross-sections are presented. It can be observed that

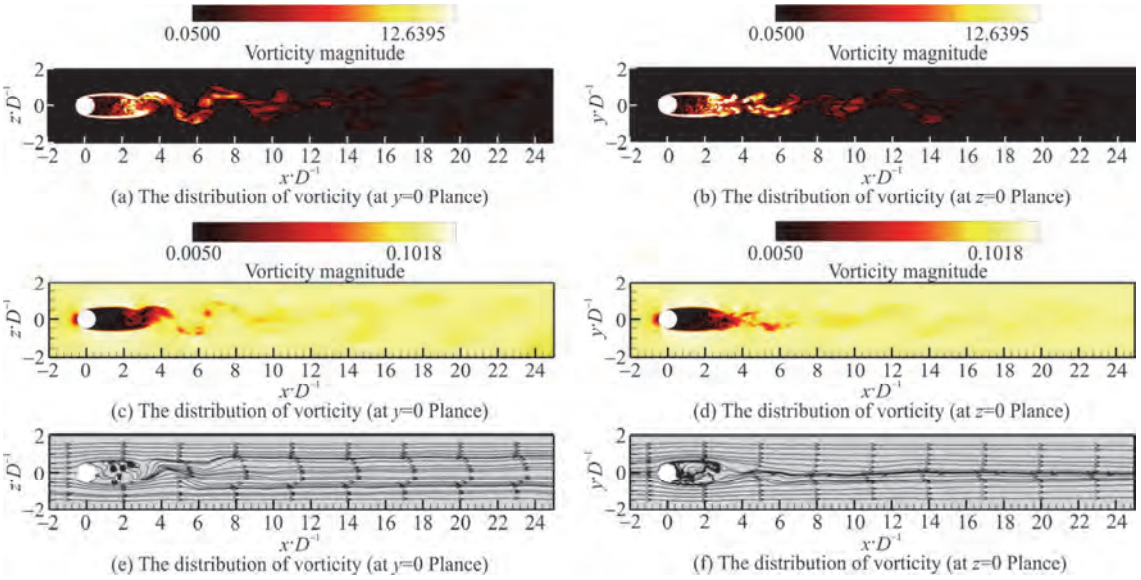

Fig. 11 (Color online) The distribution of different physical quantities (UNS)

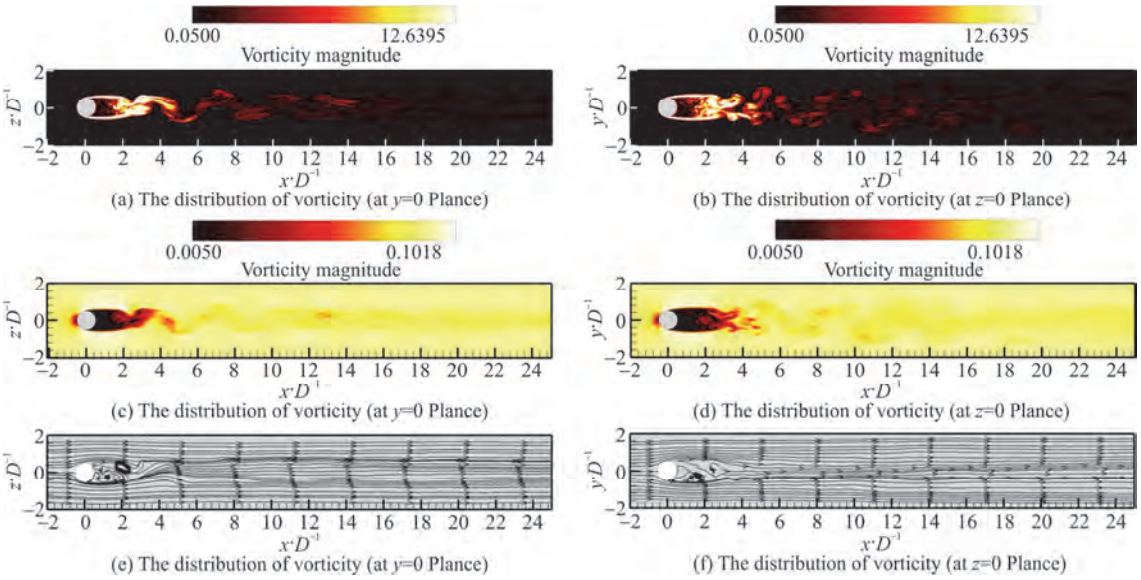

Fig. 12 (Color online) The distribution of different physical quantities $(Fr = 3)$

for velocity, vorticity and streamlines, the distribution range in the vertical direction $(y = 0)$ is smaller than that in the lateral direction $(z = 0)$. This indicates that the wake of the sphere is suppressed in the vertical direction under stratified condition. Due to this suppression, the wake develops along the lateral direction, resulting in a larger lateral dimension compared with the vertical dimension. Compared with UNS fluid, the recirculation zone in stratified fluid $(Fr = 3)$ is significantly smaller, primarily confined to $x / D < 2$.

Using the Q-criterion method, Fig. 13 illustrates the vortex structures in the wake under UNS condition. It can be observed that the vortex structures develop in all directions, exhibiting clear isotropy. As shown in Fig. 14, the vortex structures in the wake under stratified condition are presented. The location of vortex shedding is further downstream compared with UNS condition. Under stratification, the wake vortex structures undergo three stages: 3-D, non-equilibrium (NEQ), Q2D. In the near field, close to the sphere, the wake experiences weak buoyancy effects, displaying a 3-D state. As the distance from the sphere increases, density stratification begins to suppress vertical motion, transitioning the wake from a 3-D state to a NEQ state. Eventually, buoyancy fully dominates the wake flow, completely suppressing

vertical motion, and the vortex structures become flattened, entering a Q2D state.

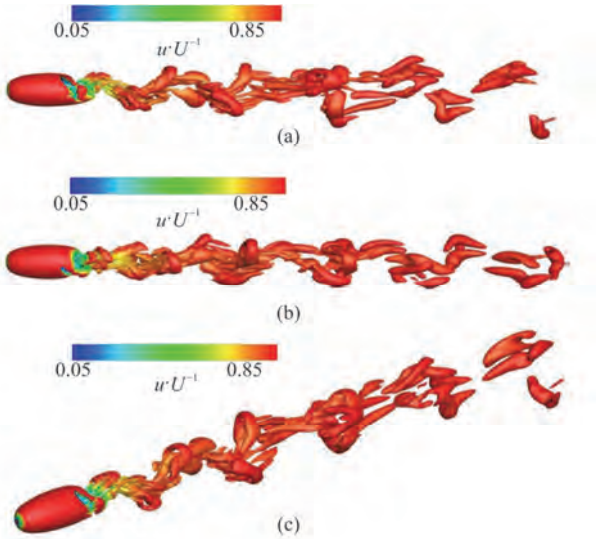

Fig. 13 (Color online) Evolution of the vortex structure in the wake (UNS)

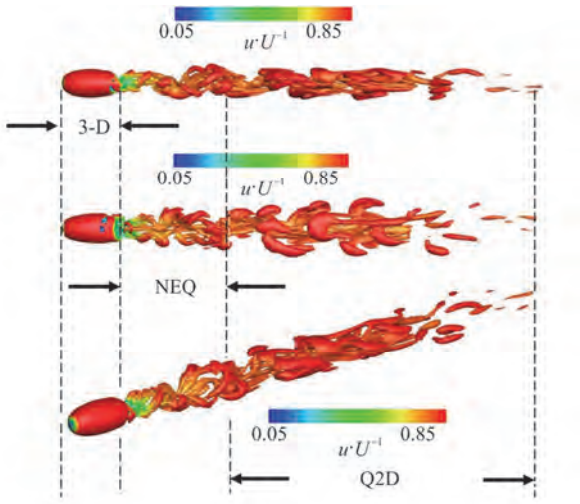

Fig. 14 (Color online) Evolution of the vortex structure in the wake $(Fr = 3)$

3.2 *The velocity deficit and the distribution of TKE*

Figure 15 shows the distribution of velocity deficit and the normalized rms velocity in different directions. Firstly, considering the velocity deficit (u/U) for UNS fluid and stratified fluid $(Fr = 3)$, the following observations are made: For the UNS fluid, the velocity deficit reaches its peak at $x/D \approx 2.7$, with $u/U > 1$, indicating the establishment of turbulence. Beyond $x/D = 2.7$, *u/U* decreases monotonically. For the stratified fluid $(Fr = 3)$, the peak is reached slightly earlier, at $x/D \approx 2.2$, with $u/U > 1$, also indicating the onset of turbulence. Between $2.2 < x/D < 7$, u/U decreases monotonically, suggesting that the wake transitions from a 3-D state to a NEQ state. After $x/D > 7$, u/U levels off, indicating that the wake has transitioned from the NEQ state to a Q2D state.

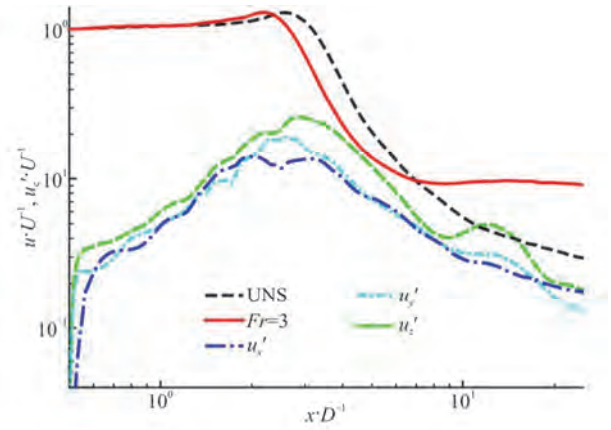

Fig. 15 (Color online) Evolution of centreline values of mean streamwise velocity deficit (u), rms velocity fluctuation (streamwise u_x', spanwise u_y', vertical u_z')

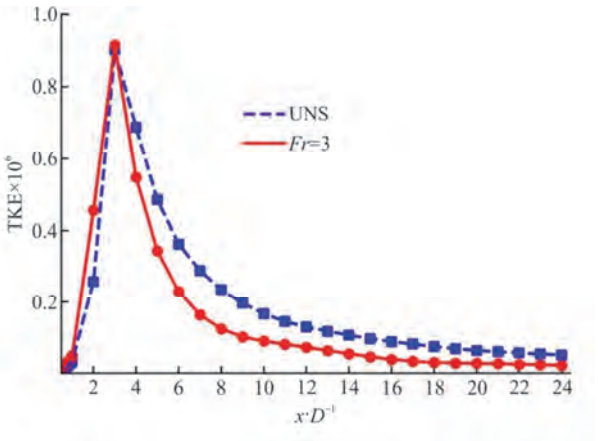

Fig. 16 (Color online) Area integrated TKE

Next, we discuss the rms velocity in different directions for the stratified fluid, as shown in Fig. 15. For $x/D < 2$, the values of u_x'/U, u_y'/U, u_z'/U are quite close, indicating isotropy in the velocity directions within the wake. For $x/D > 2$, the values of u_x'/U, u_y'/U remain relatively close, while the value of u_z'/U is significantly higher than those of u_x'/U, u_y'/U. Furthermore, within $8 < x/D < 11$, there are large oscillations in u_z'/U, indicating that for $x/D > 2$, buoyancy suppresses vertical motion in the wake and increases anisotropy.

The TKE at different positions along the wake was integrated over the area, as shown in Fig. 16. For

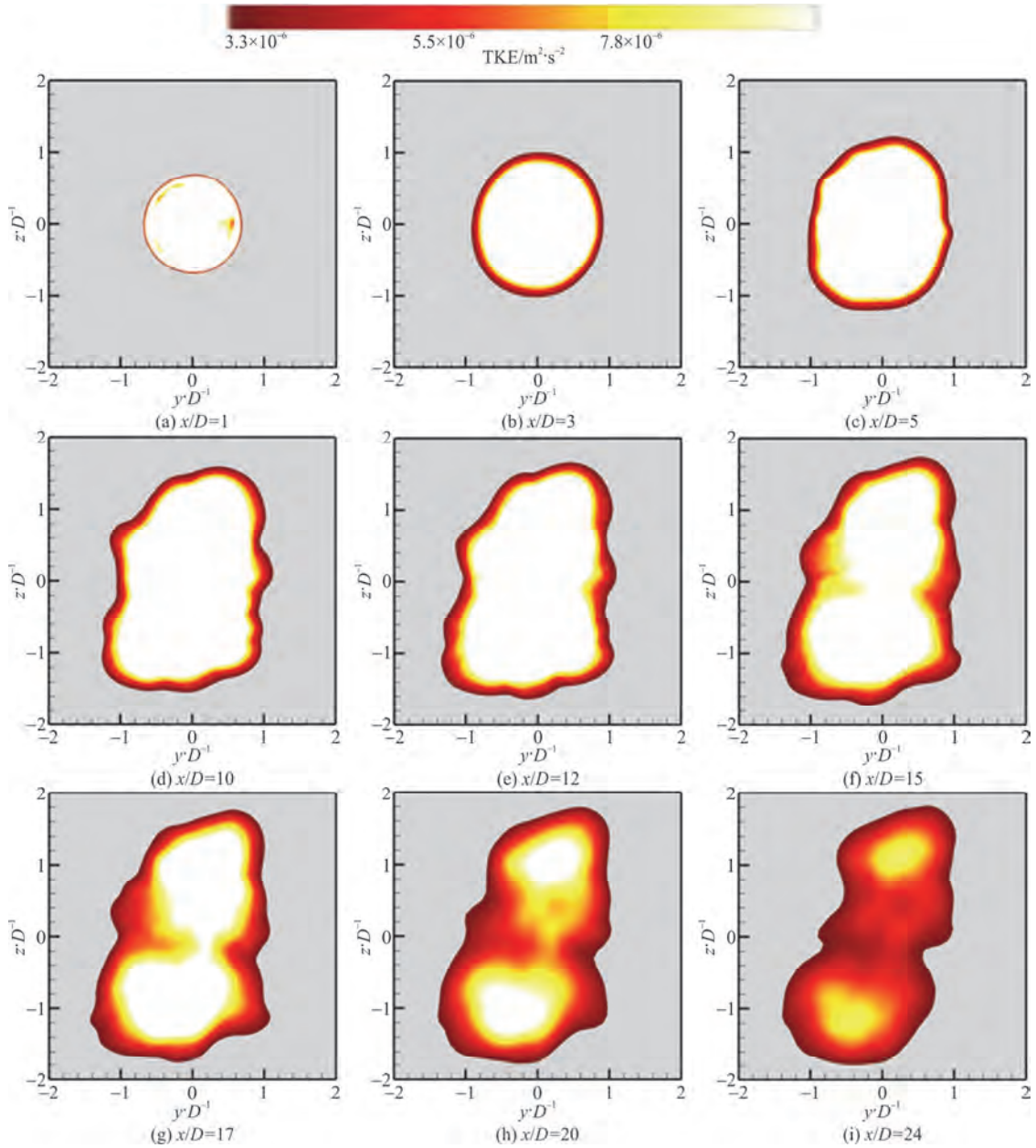

Fig. 17 (Color online) Visualization of cross-sectional contours of TKE (UNS)

both the UNS fluid and the stratified fluid $(Fr = 3)$, the TKE peaks at $x / D = 3$. For $x / D < 3$, the TKE gradually increases, with the TKE being lower in the UNS case compared with the stratified case. For $x / D > 3$, the TKE gradually decreases, with the TKE being significantly higher in the UNS case than in the stratified case.

Figures 17, 18 present the distribution of TKE under UNS and stratified conditions. In both cases, the TKE decreases gradually with increasing distance. In Fig. 17, for the UNS fluid, it is observed that as the distance increases, the shape of the TKE distribution transitions from circular to spindle-shaped, becoming wider in the vertical direction and narrower in the horizontal direction due to buoyancy effects. The vertical extent of the distribution is significantly greater than the horizontal extent. Additionally, when $x / D \geq 17$, the peak of TKE is primarily located at the upper and lower ends. In Fig. 18, for the stratified fluid $(Fr = 3)$, the distribution shape of TKE changes from an isotropic circular form to an elliptical form that is narrower in the vertical direction and wider in the horizontal direction as the distance increases. This change illustrates the suppression effect of stratification on the vertical motion of the wake. Additionally, when $x / D \geq 17$, the peak of TKE is primarily loca-

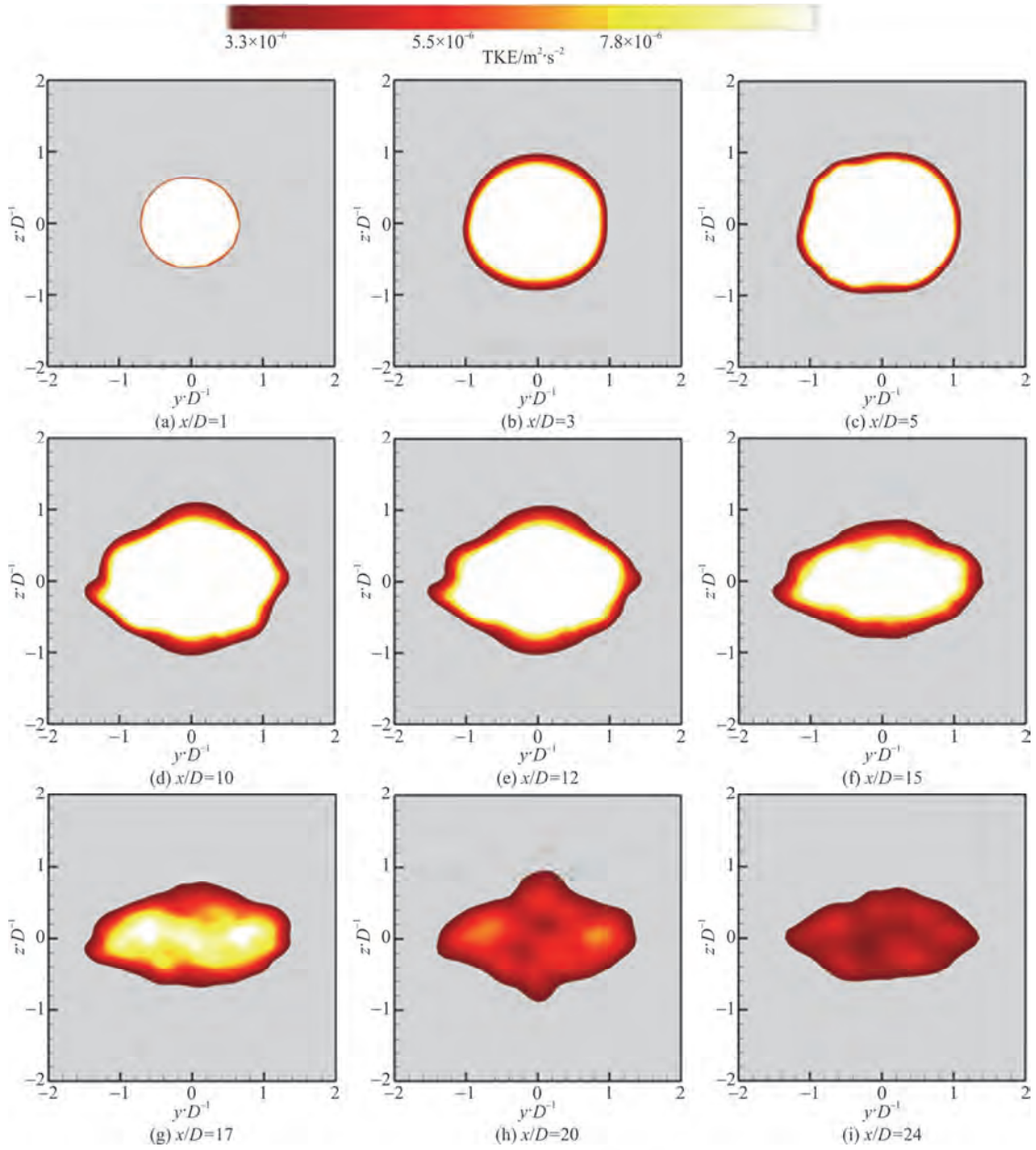

Fig. 18 (Color online) Visualization of cross-sectional contours of TKE $(Fr = 3)$

ted at the lateral ends.

3.3 *The length of wake*

In numerical simulations, the definition and measurement of wake height and wake width typically rely on the variations of certain physical quantities in the flow field, such as velocity, vorticity, or turbulence intensity[30]. In this study, the boundary region of the wake is defined where the velocity is 30% of the freestream velocity. L_V is defined as the vertical height of the wake, L_H is defined as the horizontal width of the wake. Figure 19 shows the normalized velocity deficit distribution in an UNS fluid. It can be observed that the velocity deficit distribution in the vertical direction exhibits a double-peak pattern, and within a range of $1.5L_H$, $1.5L_V$, the velocity deficit values have already approached zero. Figure 20 presents the normalized velocity deficit distribution in a stratified fluid. In this case, the velocity deficit distribution exhibits a single peak and an approximately Gaussian distribution in both the horizontal and vertical directions.

$$\rho_d = \rho - \rho_{bg} \tag{11}$$

$$\partial_z \langle \rho_d \rangle = \frac{\mathrm{d}\rho_d}{\mathrm{d}z} \tag{12}$$

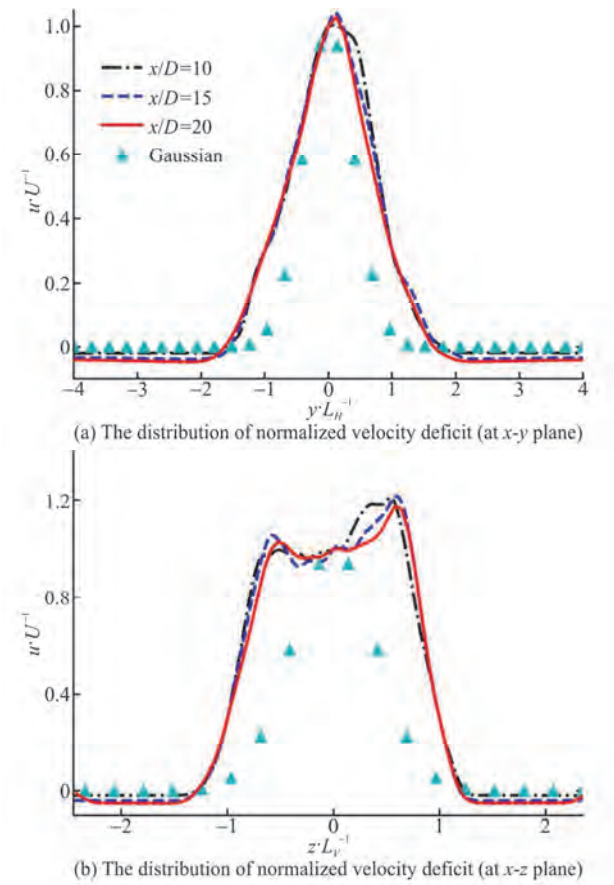

Fig. 19 (Color online) Profiles of normalized mean streamwise velocity deficit in different direction (UNS)

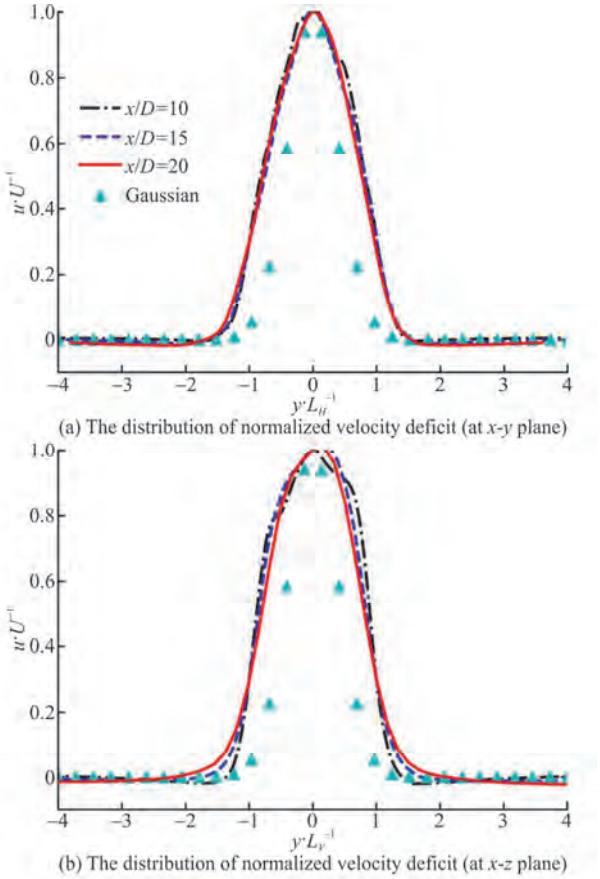

Fig. 20 (Color online) Profiles of normalized mean streamwise velocity deficit in different direction ($Fr = 3$)

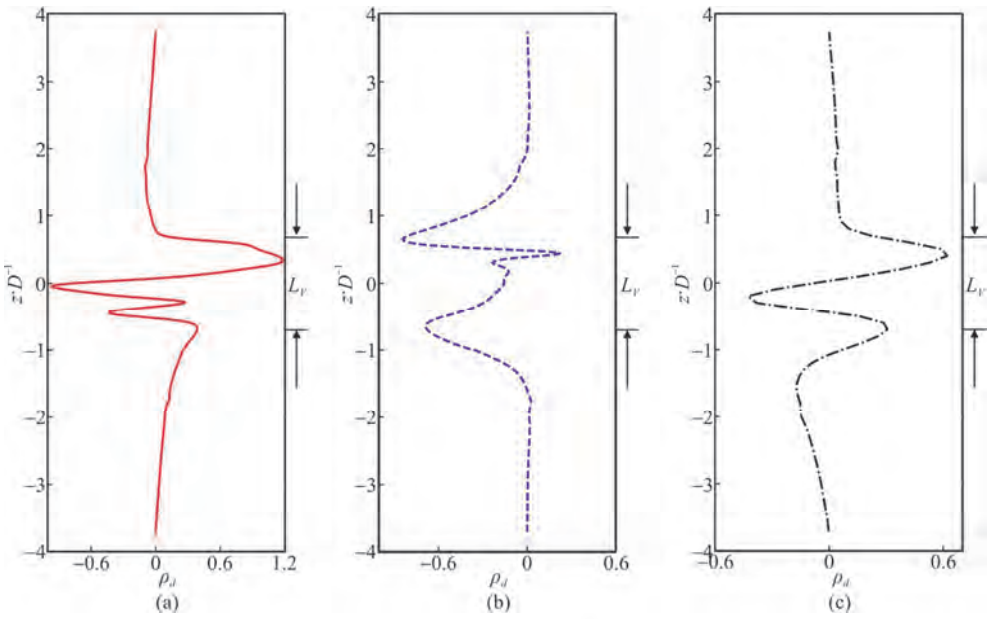

Fig. 21 (Color online) Vertical profiles of mean density deviation ($Fr = 3$)

where ρ is the vertical density, ρ_{bg} is the initial vertical density, ρ_d is the density perturbation and $\partial_z \langle \rho_d \rangle$ signifies the partial derivative of the density perturbation with respect to the vertical direction.

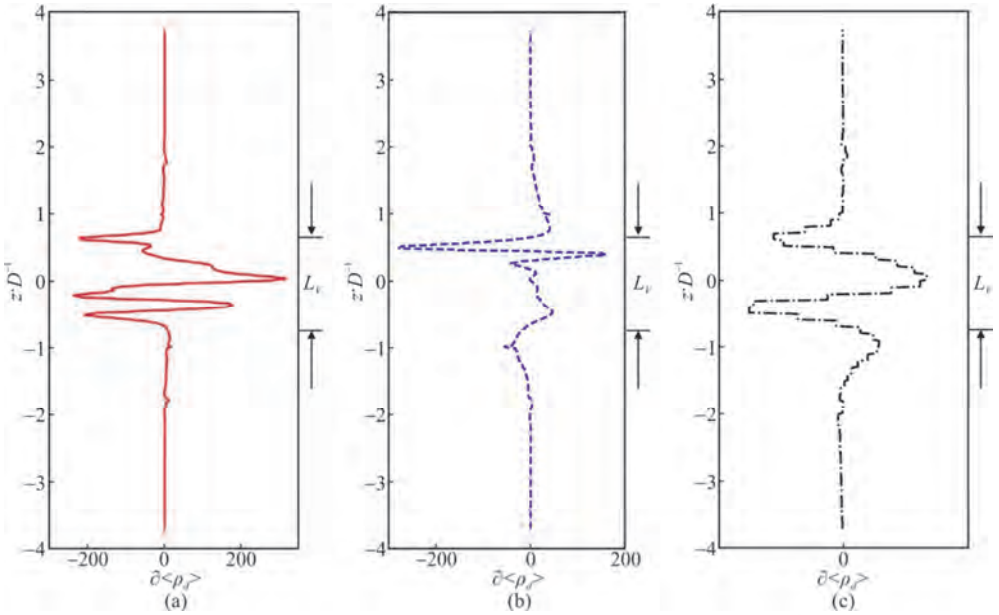

Fig. 22 (Color online) Vertical profiles of vertical gradient of mean density deviation $(Fr = 3)$

As illustrated in Figs. 21, 22, with increasing values of x/D, both ρ_d, $\partial_z\langle\rho_d\rangle$ gradually decrease. Additionally, in the vertical direction, the distribution range of ρ_d, $\partial_z\langle\rho_d\rangle$ significantly exceeds the vertical boundaries of the wake. This result is consistent with the findings of Chongsiripinyo[22].

4. Conclusions

This study employed the LES method with a temperature-dependent density model. Following the validation of the method and analysis of grid sensitivity, simulations of the flow around a sphere at a Reynolds number of 3700 were conducted under both UNS and stratified conditions $(Fr = 3)$. The comparisons focused on the horizontal and vertical vorticity, velocity, and streamline distributions. The evolution of vortex structures in the wake was also analyzed. Furthermore, the velocity deficit, rms of velocity components in all directions, and TKE distribution were quantified. Additionally, the horizontal and vertical wake lengths were examined. The main conclusions are as follows.

For a fluid with uniform density under UNS condition, a lower density results in a faster decay of the velocity deficit along the wake centerline after it reaches its peak. In contrast, in stratified fluid $(Fr = 3)$, the velocity deficit along the wake centerline initially decreases after reaching its peak but then stabilizes. On the other hand, in the UNS fluid, the velocity deficit along the wake centerline decreases monotonically after reaching its peak.

Under UNS condition, the wake's velocity, vorticity, streamlines, and vortex structures develop fully in all directions, exhibiting clear isotropy. However, under stratified conditions $(Fr = 3)$, the wake is significantly suppressed in the vertical direction. The vortex structures in the wake undergo substantial changes due to varying buoyancy effects with distance, which can be categorized into three stages: 3-D, NEQ, Q2D.

In stratified condition $(Fr = 3)$, the rms of velocity components in different directions shows that for $X/D < 2$, the values of u_x'/U, u_y'/U, u_z'/U are quite similar. However, due to the influence of buoyancy, the value of u_z'/U becomes significantly larger than those of u_x'/U, u_y'/U. For $X/D > 3$, the TKE of the UNS wake exceeds that of the stratified wake. The TKE distribution in UNS condition forms a spindle shape, being wider vertically and narrower horizontally. In contrast, the TKE distribution in stratified conditions forms an elliptical shape, being narrower vertically and wider horizontally.

Under UNS condition, the velocity deficit in the wake exhibits a bimodal distribution in the vertical direction. In contrast, under stratified conditions $(Fr = 3)$, the velocity deficit shows a near-Gaussian distribution in both the horizontal and vertical directions. Along the vertical direction, the distribution ranges of both the density perturbation and its partial derivative are significantly larger than that of the wake.

Acknowledgment

This research received other funding agency in the public, commercial, or not-for-profit sectors.

Compliance with ethical standards

Conflict of interest: The authors declare that they have no conflict of interest. Liu-shuai Cao, De-cheng Wan are editorial board members for the Journal of Hydrodynamics and was not involved in the editorial review, or the decision to publish this article. All authors declare that there are no other competing interests.

Ethical approval: This article does not contain any studies with human participants or animals performed by any of the authors.

Informed consent: Not application.

References

[1] Cao L. S., Huang F. L., Liu C. et al. Vortical structures and wakes of a sphere in homogeneous and density stratified fluid [J]. *Journal of Hydrodynamics*, 2021, 33(2): 207-215.

[2] Cao L., Pan Y., Gao G. et al. Review on the hydro-and thermo-dynamic wakes of underwater vehicles in linearly stratified fluid [J]. *Journal of Marine Science and Engineering*, 2024, 12(3): 490.

[3] Gao G., Pan Y., Wang Y. et al. Evolution and propagation characteristics of the wake induced by an underwater vehicle moving in two layers of fluid: A parametric study [J]. *Physics of Fluids*, 2024, 36(11): 112125.

[4] Bonnier M., Eiff O. Experimental investigation of the collapse of a turbulent wake in a stably stratified fluid [J]. *Physics of Fluids*, 2002, 14(2): 791-801.

[5] Lin Q., Boyer D. L., Fernando H. J. S. Turbulent wakes of linearly stratified flow past a sphere [J]. *Physics of Fluids A: Fluid Dynamics*, 1992, 4(8): 1687-1696.

[6] Lin Q., Lindberg W. R., Boyer D. L. et al. Stratified flow past a sphere [J]. *Journal of Fluid Mechanics*, 1992, 240: 315-354.

[7] Kim H. J., Durbin P. A. Observations of the frequencies in a sphere wake and of drag increase by acoustic excitation [J]. *Physics of Fluids*, 1988, 31(11): 3260-3265.

[8] Xiang X., Chen K., Madison T. et al. Experiments and simulations of low Re sphere wakes with and without stratification [C]. *Proceedings of the Eighth International Symposium on Stratified Flows*, San Diego, USA, 2016.

[9] Xiang X., Madison T. J., Sellappan P. et al. The turbulent wake of a towed grid in a stratified fluid[J]. *Journal of Fluid Mechanics*, 2015, 775: 149-177.

[10] Huang F., Meng Q., Cao L. et al. Wakes and free surface signatures of a generic submarine in the homogeneous and linearly stratified fluid [J]. *Ocean Engineering*, 2022, 250: 111062.

[11] Wang C., Xu D., Gao J. et al. Numerical study of surface thermal signatures of lee waves excited by moving underwater sphere at low Froude number [J]. *Ocean Engineering*, 2021, 235: 109314.

[12] Wang C., Zhang H., Zhu H. Numerical predictions of internal waves and surface thermal signatures by underwater vehicles in density-stratified water using OpenFOAM [J]. *Ocean Engineering*, 2023, 272: 113847.

[13] Nadaf E., Brown J. M., Radko T. Turbulent wakes in a non-uniformly stratified environment [J]. *Physics of Fluids*, 2022, 34(10): 105123.

[14] Jacobs C. T. Modelling a moving propeller system in a stratified fluid using OpenFOAM [J]. *Fluids*, 2020, 5(4): 217.

[15] Chen Q., Lin Q., Xuan Y. et al. Investigation on the thermohaline structure of the stratified wake generated by a propagating submarine [J]. *International Journal of Heat and Mass Transfer*, 2021, 166: 120808.

[16] Rodríguez I., Lehmkuhl O., Borrell R. et al. Flow dynamics in the turbulent wake of a sphere at sub-critical Reynolds numbers [J]. *Computers and Fluids*, 2013, 80: 233-243.

[17] Rodriguez I., Borell R., Lehmkuhl O. et al. Direct numerical simulation of the flow over a sphere at *Re* = 3 700 [J]. *Journal of Fluid Mechanics*, 2011, 679: 263-287.

[18] Constantinescu G., Squires K. Numerical investigations of flow over a sphere in the subcritical and supercritical regimes [J]. *Physics of Fluids*, 2004, 16(5): 1449-1466.

[19] Chongsiripinyo K., Sarkar S. Stratified turbulence in disk wakes [C]. *Proceedings of the Eleventh International Symposium on Turbulence and Shear Flow Phenomena (TSFP-11)*, Southampton, UK, 2019.

[20] Chongsiripinyo K., Sarkar S. Effect of stratification on the turbulent wake behind a sphere at *Re* = 10 000 [C]. *Tenth International Symposium on Turbulence and Shear Flow Phenomena (TSFP10)*, Chicago, USA, 2017.

[21] Chongsiripinyo K., Sarkar S. Decay of turbulent wakes behind a disk in homogeneous and stratified fluids [J]. *Journal of Fluid Mechanics*, 2020, 885: A31.

[22] Chongsiripinyo K. The downstream of a density-stratified sphere wake [J]. *Engineering Journal*, 2021, 25(5): 1-12.

[23] Chongsiripinyo K., Pal A., Sarkar S. On the vortex dynamics of flow past a sphere at *Re* = 3 700 in a uni-formly stratified fluid [J]. *Physics of Fluids*, 2017, 29(2): 020704.

[24] Pal A., Chongsiripinyo K., Sarkar S. Dynamics of flow over a sphere at *Re* = 3 700 in moderate to highly stratified environments [C]. *Proceedings of the Eighth International Symposium on Stratified Flows*, San Diego, USA, 2016.

[25] Pal A., Sarkar S., Posa A. et al. Direct numerical simulation of stratified flow past a sphere at a subcritical Reynolds number of 3700 and moderate Froude number [J]. *Journal of Fluid Mechanics*, 2017, 826: 5-31.

[26] Ortiz-Tarin J. L., Nidhan S., Sarkar S. The high-Reynolds-number stratified wake of a slender body and its comparison with a bluff-body wake [J]. *Journal of Fluid Mechanics*, 2023, 957: A7.

[27] Ohh C. Y., Spedding G. R. The effects of stratification on the near wake of 6: 1 prolate spheroid [J]. *Journal of Fluid Mechanics*, 2024, 997: A43.

[28] Zhou Q. Mixing in a strongly stratified turbulent wake quantified by bulk and conditional statistics [J]. *Journal of Fluid Mechanics*, 2024, 997: A41.

[29] van Dine A., Pham H. T., Sarkar S. Turbulent shear layers in a uniformly stratified background: DNS at high Reynolds number [J]. *Journal of Fluid Mechanics*, 2021, 916: A42.

[30] Orr T. S., Domaradzki J. A., Spedding G. R. et al. Numerical simulations of the near wake of a sphere moving in a steady, horizontal motion through a linearly stratified fluid at *Re* = 1 000 [J]. *Physics of Fluids*, 2015, 27(3): 035113.